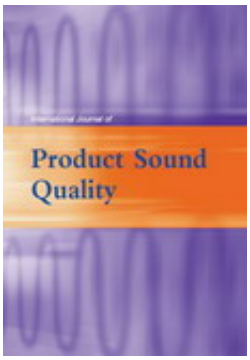

International Journal of Product Sound Quality

ISSN online: 1742-6766 - ISSN print: 1742-6758
https://www.inderscience.com/ijpsq

Design and modelling of a portable ultrasonic cleaner

Qihan Zheng, Jinyang Xu, Xingjian Shi, Yiyun Yu

DOI: 10.1504/IJPSQ.2022.10047180

Article History:

Received:	23 March 2022
Accepted:	04 April 2022
Published online:	28 September 2023

Design and modelling of a portable ultrasonic cleaner

Qihan Zheng, Jinyang Xu*, Xingjian Shi and Yiyun Yu

School of Mechanical Engineering,
Shanghai Jiao Tong University,
Shanghai 200240, China
Email: freedogi@sjtu.edu.cn
Email: xujinyang@sjtu.edu.cn
Email: shixingjian@sjtu.edu.cn
Email: yyy520503@sjtu.edu.cn
*Corresponding author

Abstract: In view of the shortcomings of the existing kitchen ultrasonic cleaning equipment, this paper designs a portable ultrasonic cleaner, which is free of installation on the basis of meeting the daily cleaning needs of the kitchen. The cleaner specifically includes an ultrasonic transducer group, a waterproof sealed box, and a control system. During the working operation, continuous high-frequency electrical excitations are generated through the power supply circuit and control circuit in the master control box. Then the ultrasonic signals are generated through the electromechanical conversion of the transducer group and transmitted to the sink through the shell. Additionally, the equipment uses the cavitation effects caused by ultrasonic waves to clean stains. This paper determines the appropriate size of the transducer through theoretical calculations and uses the finite element simulation to verify its performance parameters. Finally, the COMSOL multi-physics coupling analysis was carried out to obtain the sound pressure level distribution generated by the device in the sink to validate the cleaning performance of the designed equipment.

Keywords: ultrasonic cleaning; ultrasonic transducer; finite element simulation; multi-physics coupling analysis.

Reference to this paper should be made as follows: Zheng, Q., Xu, J., Shi, X. and Yu, Y. (2023) 'Design and modelling of a portable ultrasonic cleaner', *Int. J. Product Sound Quality*, Vol. 1, No. 1, pp.3–17.

Biographical notes: Qihan Zheng obtained his Bachelor's degree from the Shanghai Jiao Tong University, China in 2021. His main speciality is mechanical engineering.

Jinyang Xu is an Associate Professor at the Shanghai Jiao Tong University, China. His research interests are composites machining, numerical modelling, micro/nano cutting, and surface texturing. He is currently serving as the Editor-in-Chief of the *Journal of Coating Science and Technology* and the *International Journal of Product Sound Quality*. He is also an associate editor of *Simulation – Transactions of the Society for Modeling and Simulation International*.

Xingjian Shi obtained his Bachelor's degree from the Shanghai Jiao Tong University, China in 2021. His main speciality is nuclear engineering and technology.

Yiyun Yu obtained his Bachelor's degree from the Shanghai Jiao Tong University, China in 2021. His main speciality is energy and power engineering.

1 Introduction

Ultrasonic cleaning equipment uses the local high temperature and high pressure generated by the ultrasonic cavitation effect, which can effectively peel off the stubborn stains on the surface of the object to be washed (Lin, 2009). In terms of kitchen use, because of its strong ability to decompose and strip oil and no dead ends, ultrasonic cleaning has broad application prospects (Chang, 2017).

The traditional ultrasonic cleaning machine needs to remove all the original cleaning tanks in the kitchen for the installation, which takes up a lot of space. And it is complicated for installation, difficult to maintain, consuming a lot of power, and impossible to install at the bottom of some small kitchen sinks. As for the small input ultrasonic cleaning machine consisting of only one or two transducers, it is small in size, but its cleaning efficiency is low, and the cleaning range is also limited. According to Li (2019), such a cleaner will be helpless when encountering stubborn stains that are difficult to clean. Aiming at addressing deficiencies of existing products in the market, this article developed a portable wall-mounted ultrasonic cleaning machine, which is characterised by being hung on the side wall of the sink and generating ultrasonic waves to clean the items in the tank. Compared with the installed cleaning system, the cleaning machine occupies a small space, does not require installation, and is easy to use. It can deal with large kitchen sinks and stubborn kitchen stains. According to Gonzalez-Avila et al. (2012), the multi-transducer design of the cleaning machine can ensure a good cleaning range and cleaning efficiency.

The cleaning machine specifically includes a group of ultrasonic transducers, a waterproof sealed housing, and a control system. Firstly, according to the market research and literature survey, the transducer frequency was determined as 40 kHz, which suits for ultrasonic cavitation effect (Fu et al., 2015). Secondly, according to the principle and structural characteristics of the piezoelectric ultrasonic transducer, the electromechanical equivalent method was used to obtain the transducer. The size selection formula is combined with the actual requirements to design the size of the transducer material. Then the simulations were performed to obtain various parameters of the transducer to check whether its performance meets expectations. Finally, the COMSOL Multiphysics software was used to simulate the sound field generated by the entire ultrasonic cleaning machine in the sink to verify the cleaning effect of the whole machine (Kim and Kim, 2014).

2 The design procedures

2.1 The structure design of the whole machine

To maximise the cleaning efficiency while reducing the total size and weight as much as possible, a cross-connected form of five ultrasonic transducers was selected, glued, and packaged in a sealed box. The engineering drawing of the transducer group and the waterproof sealed enclosure is shown in Figure 1. The vibrating surface of the front vibrating plate of the transducer is glued to the inside of the front plate of the sealed box made of TC4 alloy, and ultrasonic waves are generated and transmitted to the water tank through the front plate to produce an ultrasonic cavitation effect for cleaning. A guiding tube extends from the top of the sealed box, which connects the power supply circuit and the control circuit.

Figure 1 The engineering drawing of the portable ultrasonic cleaner

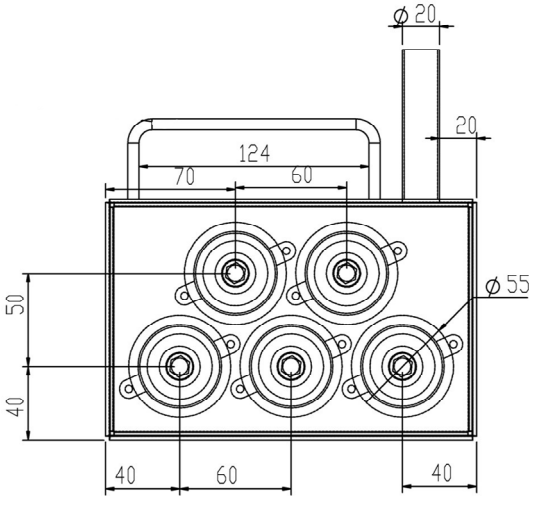

2.2 Design of the ultrasonic transducer

The structure of the first-order longitudinal vibration piezoelectric transducer is shown in Figure 2. It is stacked by the front radiation head (front cover), piezoelectric ceramic chipset, and rear mass (rear cover). To ensure a close fit, pre-stressed bolts are generally inserted.

The front cover is regarded as a one-dimensional variable cross-section rod. According to Xu et al. (2018), considering the simple harmonic vibration in the thickness direction, the vibration equation can be expressed as follows.

$$\frac{\partial^2 z}{\partial x^2}+\frac{1}{S}\cdot\frac{\partial S}{\partial x}\cdot\frac{\partial z}{\partial x}+k^2 z=0 \tag{1}$$

According to the idea of electromechanical equivalent, the equivalent impedance diagram of the variable cross-section rod can be obtained, as shown in Figure 3.

Figure 2 The structure of the piezoelectric transducer (see online version for colours)

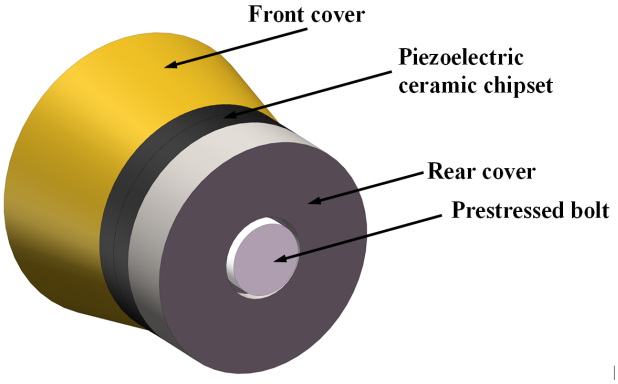

Figure 3 The equivalent impedance diagram of the one-dimensional variable cross-section rod

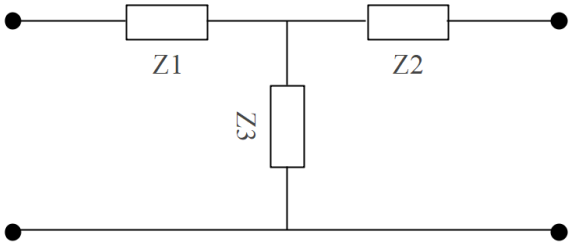

Using the solution of the vibration equation, the equivalent impedance formula of the front cover can be obtained (related to the density and Young's modulus of the material):

$$Z_{f1} = -\frac{i\rho_1 c_1 S_2}{k_1 l_1}\left(\sqrt{\frac{S_1}{S_2}} - 1\right) - i\rho_1 c_1 S_2 \cot k_1 l_1 + \frac{i\rho_1 c_1 \sqrt{S_1 S_2}}{\sin k_1 l_1} \tag{2}$$

$$Z_{f2} = -\frac{i\rho_1 c_1 S_2}{k_1 l_1}\left(\sqrt{\frac{S_1}{S_2}} - 1\right) - i\rho_1 c_1 S_1 \cot k_1 l_1 + \frac{i\rho_1 c_1 \sqrt{S_1 S_2}}{\sin k_1 l_1} \tag{3}$$

$$Z_{f3} = \frac{\rho_1 c_1 \sqrt{S_1 S_2}}{i \sin k_1 l_1} \tag{4}$$

where ρ_1, c_1, S_1, l_1, k_1 are respectively the material density of the front cover, the speed of sound, the cross-sectional area of the radiating surface, the length and the wave number.

The back cover is relatively simple and can be regarded as a cylinder with a constant cross-section. It is equivalent to $Z_1 = Z_2$ in the one-dimensional variable cross-section rod impedance diagram (Xu and Cheng, 2020), and the cross-sectional areas of the front and back ends are equal, set to S_2, and the simplified equivalent impedance expression is obtained:

$$Z_{b1} = Z_{b2} = i\rho_2 c_2 S_2 \tan\left(\frac{k_2 l_2}{2}\right), Z_{b3} = \frac{\rho_2 c_2 S_2}{i \sin k_2 l_2} \tag{5}$$

where ρ_2, c_2, S_2, l_2, k_2 are the material density of the back cover, the speed of sound, the cross-sectional area of the radiating surface, the length and the wave number, respectively.

Piezoelectric ceramic chipset is an electromechanical coupling element. In addition to elastic mechanical impedance in its equivalent impedance diagram, there is also an electromechanical conversion impedance, which converts the applied voltage into a mechanical boundary form. According to Shi and Yang (2011), the equivalent circuit of the piezoelectric ceramic chipset can be depicted in Figure 4.

Figure 4 The equivalent circuit diagram of the piezoelectric ceramic crystal stack

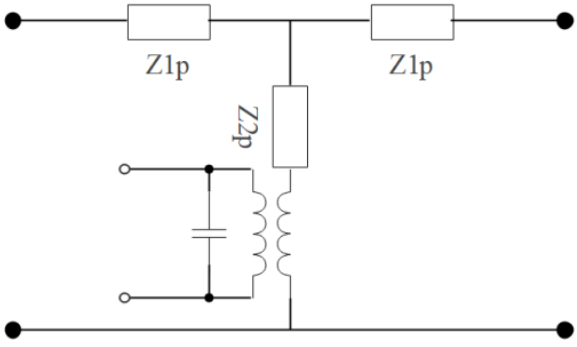

The calculated equivalent impedance of the piezoelectric ceramic crystal stack is as follows.

$$Z_{1p} = i\rho_p c_p S_p \frac{\tan k_p l_p}{2}, Z_{2p} = \frac{\rho_p c_p S_p}{i \sin k_p l_p} \tag{6}$$

where ρ_p, c_p, S_p, l_p, k_p are respectively the density, sound velocity, cross-sectional area, length and wave number of the piezoelectric ceramic sheet.

In the design and calculation of the transducer, the nodal plane is an essential concept. To maximise the amplitude of the two ends of the transducer in the resonance state, i.e., most of the ultrasonic energy is radiated from the front and rear cover plates, the length of the transducer needs to be designed to be the half-wavelength of the longitudinal wave (Fu et al., 2014). Under this condition, there must be a cross-section in the middle of the transducer that has a displacement of 0, and this cross-section is called the nodal surface. According to Zhang (2009), the frequency equations can be expressed separately for the quarter-wavelength parts on both sides of the nodal surface, and the frequency equation of the entire transducer can be obtained as follows.

$$\begin{aligned} \tan k_p l_{p2} &= \frac{\rho_p c_e S_p}{X_{m2}} = \frac{\rho c_p S}{\rho_2 c_2 S_2} \cot k_2 l_2 \\ &= \frac{\rho c_p S}{\rho_2 c_2 S_1} \cdot \frac{F k_2 l_2 \left[\tan k_2 l_2 - k_2 l_2 (F+1)\right]}{k_2 l_2 - \left[1 + k_2^2 l_2^2 F(F+1)\right] \tan k_2 l_2} \end{aligned} \tag{7}$$

The vibration speed ratio (η) of the transducer can be denoted as follows.

$$\eta = -\frac{\cos k_2 l_2 \left[z_p \tan\left(\frac{k_p l_p}{2}\right) + z_2 \tan k_2 l_2 \right]}{\frac{F}{F+1} \cdot \frac{z_1}{\sin k_1 l_1} + \left(\frac{F+1}{F} \cos k_1 l_1 - \frac{\sin k_1 l_1}{F k_1 l_1} \right) \left[z_p \tan\left(\frac{k_p l_p}{2}\right) - \frac{z_2}{F k_1 l_1} - z_2 \cot k_1 l_1 \right]} \quad (8)$$

where $z_1 = \rho_1 c_1 S_1$, $z_2 = \rho_2 c_2 S_2$, $z_p = \rho_p c_p S_p$.

In order to verify whether the product meets the requirements, the following constraints and objectives are set, as shown in Table 1.

Table 1 The main constraints and objectives

Features	*Parameters*
Size of control box	200 × 180 × 75 mm^3
Size of transducer box	180 × 50 × 100 mm^3
Ultrasonic frequency	40 kHz
Power	300 W
Voltage	AC 220 V
Size of applicable sink	Length + width < 80 cm
Time to clean	Bowls 12 min/fruits and vegetables 5 min/customisable
Length of wire	1.5 m

The most reasonable size configuration scheme can be calculated, as shown in Figure 5.

Figure 5 The size configuration scheme

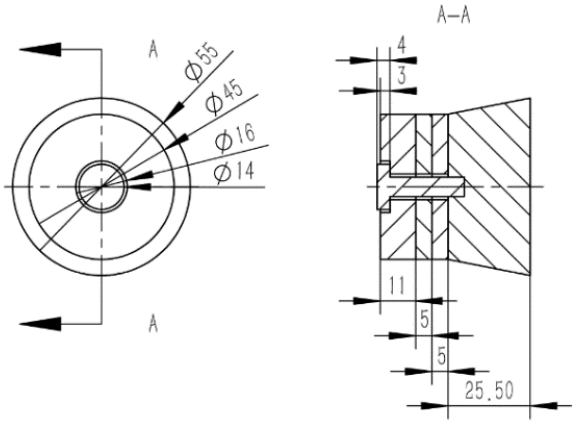

2.3 Finite element analysis and validation of a single transducer

The finite element analysis software ANSYS can be used to analyse the natural frequency, electromechanical conversion efficiency, and electroacoustic characteristics of a transducer (Li et al., 2016). A half-section of the transducer is intercepted, and a two-dimensional axisymmetric model is established for finite element analysis.

As a typical electromechanical conversion element, the piezoelectric crystal not only has its own electrical properties (dielectric constant) and mechanical properties (material

stiffness), but also contains an organic electrical coupling component to reflect the electromechanical conversion characteristics (Mo, 2007). According to Duan et al. (2018), the generalised matrices and generalised vectors used in the analysis of piezoelectric coupling problems, as well as the governing equations, can be expressed as follows.

$$\begin{bmatrix}[M] & [0]\\ [0] & [M]\end{bmatrix}\begin{Bmatrix}\{\ddot{u}\}\\ \{\ddot{V}\}\end{Bmatrix}+\begin{bmatrix}[C] & [0]\\ [0] & [0]\end{bmatrix}\begin{Bmatrix}\{\dot{u}\}\\ \{\dot{V}\}\end{Bmatrix}+\begin{bmatrix}[K] & [K^Z]\\ [K^Z]^T & [K^d]\end{bmatrix}\begin{Bmatrix}\{u\}\\ \{V\}\end{Bmatrix}=\begin{Bmatrix}\{F\}\\ \{Q\}\end{Bmatrix} \tag{9}$$

For the transducer model, since its key components are composed of rotating bodies and have good symmetry, it was considered to establish an axisymmetric quasi-physical model, which can change from three-dimensional analysis to two-dimensional analysis, and the modelling complexity is significantly reduced. The electrode sheet, adhesive layer, decoupling gasket, and M8 threaded hole on the front radiator head between the piezoelectric ceramics were ignored. These structures have little effect on the result. Secondly, each part of the transducer was regarded as a continuum. When analysing electroacoustic and vibration characteristics, the influence of pre-stressing was ignored.

Figure 6 The geometric model of the designed transducer (see online version for colours)

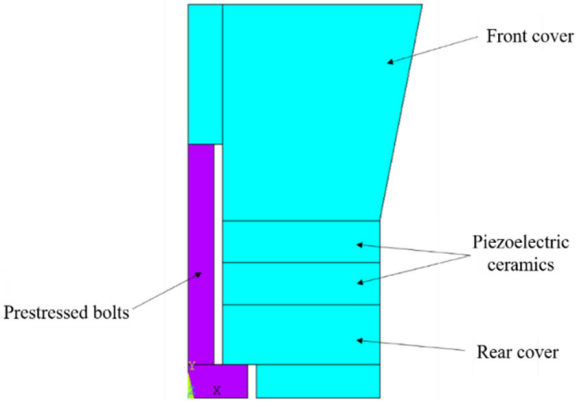

Additionally, a two-dimensional axisymmetric model was used for analysis. The element selection of the finite element model is shown in Table 2. The PLANE13 element is a two-dimensional four-node element, which can analyse magnetic, thermal, electrical, piezoelectric, and structural fields. According to Zhang et al. (2020), it can realise the coupling analysis of the two physical fields. PLANE182 element is a two-dimensional four-node element, which is a pure solid element and can be used to analyse plane stress and strain problems.

Table 2 The unit type definition

Unit type	*Internal options*
PLANE13	Axisymmetric
	Freedom UX, UY, VOLT
PLANE182	Axisymmetric

During the analysis of the transducer, the elastic characteristics and damping characteristics of the metal cover, pres-tressed bolts, and piezoelectric ceramics need to be considered. The material of the rear cover plate was set to #45 steel, the material of the front cover plate was set to 1A50 aluminium, and the material of the pre-stressing bolt was set to #45 steel, as shown in Table 3.

Table 3 Mechanical parameters of the metal parts

Part name	*Material*	*Density kg/m³*	*Young's modulus GPa*	*Poisson's ratio*
Front cover	1A50 aluminium	2,790	71.5	0.34
Rear cover	#45 steel	7,850	209	0.269
Pre-stressed bolt	#45 steel	7,850	209	0.269

For the mechanical parameters of anisotropic piezoelectric ceramics, it is necessary to use the stiffness matrix [*C*] to express them. The density and stiffness matrices of PZT-4 piezoelectric ceramics are as follows:

- Density: ρ = 7,500 kg/m³.
- Stiffness matrix:

$$[C] = \begin{bmatrix} C_{11} & C_{12} & C_{13} & & & & \\ C_{21} & C_{22} & C_{23} & & & & \\ C_{31} & C_{32} & C_{33} & & & & \\ & & & C_{66} & & & \\ & & & & C_{44} & & \\ & & & & & C_{44} & \end{bmatrix}$$

$$= \begin{bmatrix} 13.9 & 7.78 & 7.43 & & & & \\ 7.78 & 13.9 & 7.43 & & & & \\ 7.43 & 7.43 & 11.5 & & & & \\ & & & 3.06 & & & \\ & & & & 2.56 & & \\ & & & & & 2.56 & \end{bmatrix}$$

The PZT-4 piezoelectric ceramic dielectric constant matrix used in this modal analysis is as follows:

$$\varepsilon^s = \begin{bmatrix} 0.646 & & \\ & 0.646 & \\ & & 0.562 \end{bmatrix} * 10^{-8} F / m$$

$$\frac{\varepsilon^s}{\varepsilon_0} = \begin{bmatrix} 730 & & \\ & 730 & \\ & & 635 \end{bmatrix}$$

According to Wang and Du (2019), the e-type equation and the e-constant matrix are input. The order of the general parameter matrix is XX, YY, ZZ, YZ, XZ, XY, and the coordinate arrangement in the ANSYS software is XX, YY, ZZ, XY, YZ, XZ, so the last three rows and the last three columns need to be changed. The e-type parameter matrix should be in the form of 6 × 3.

$$e = \begin{bmatrix} & & e_{31} \\ & & e_{31} \\ & & e_{31} \\ & & 0 \\ e_{15} & & \\ & e_{15} & \end{bmatrix} = \begin{bmatrix} & & -5.2 \\ & & -5.2 \\ & & 15.1 \\ & & 0 \\ 12.7 & & \\ & 12.7 & \end{bmatrix}$$

After completing the definition of material parameters, it is necessary to divide the geometric model into blocks. Firstly, each part of the model is cut into quadrilaterals. Then the edge of each quadrilateral was divided manually. To ensure that the mapped mesh can be obtained, the number of divisions on the sides should be consistent. From the model size, a reasonable element size of about 0.5 mm was selected. The meshing method was chosen as mapped.

The analysis type was selected as modal and the number of modes to be solved was set to 6, indicating that the first six modes are extracted.

When the piezoelectric wafer receives electrical energy and converts it into mechanical energy through the inverse piezoelectric effect, the loss will inevitably occur, the mechanical energy generated will not all be converted into ultrasonic vibration, but a part of it will generate heat and escape through friction (Wang and Chen, 2018). The definition of the mechanical quality factor is:

$$Q_m = \frac{2\pi E_0}{E_1} \tag{13}$$

In the formula, E_0 represents the mechanical energy stored by the transducer vibrator, and E_1 represents the mechanical energy lost due to factors such as friction in each vibration cycle.

Since the stored mechanical energy and the lost mechanical energy are difficult to measure, the mechanical quality factor of an ultrasonic transducer is generally calculated indirectly by measuring its –3 db bandwidth (Hu et al., 2021). The resonance frequency f_0 and the bandwidth Δf were used to calculate the mechanical quality factor.

$$Q_m = \frac{f_0}{\Delta f} = \frac{f_0}{f_2 - f_1} \tag{14}$$

The electromechanical coupling coefficient is defined under ideal conditions. In this case, the unconverted electric energy is not lost but is stored in elastic energy or dielectric mode (Ma et al., 2017). This parameter describes the strength of the transducer's ability to convert electrical energy into mechanical energy. The definition is as follows:

$$k_{eff} = \frac{U_I}{\sqrt{U_M U_E}} \tag{15}$$

where U_I is the interaction energy density. U_M is the elastic energy density, and U_E is the dielectric energy density.

The anti-resonant frequency f_a of the transducer is near the maximum impedance frequency and is the operating frequency in the receiving state. The calculation formula of the electromechanical coupling coefficient is as follows:

$$k_{eff} = \sqrt{1 - \frac{f_r^2}{f_a^2}} \tag{16}$$

where f_r is the resonance frequency of the transducer.

2.4 Analysis of the sound field of the washing machine in the washing tank

The main principle of ultrasonic cleaning is the ultrasonic cavitation effect. The sound pressure at the cavitation nucleus generated by the ultrasonic vibration radiated into the cleaning liquid is directly related to the quality of the ultrasonic cavitation effect. Therefore, according to Fan et al. (2021), the sound field should be distributed as evenly as possible in the cleaning tank, and the sound pressure level should be as large as possible so as to ensure the cleaning effect.

Additionally, through the use of COMSOL, the numerical simulation calculation can be easily carried out (Fu et al., 2018). The modelling of the washing machine and the water body is shown in Figure 7.

Figure 7 The washing machine and the water body (see online version for colours)

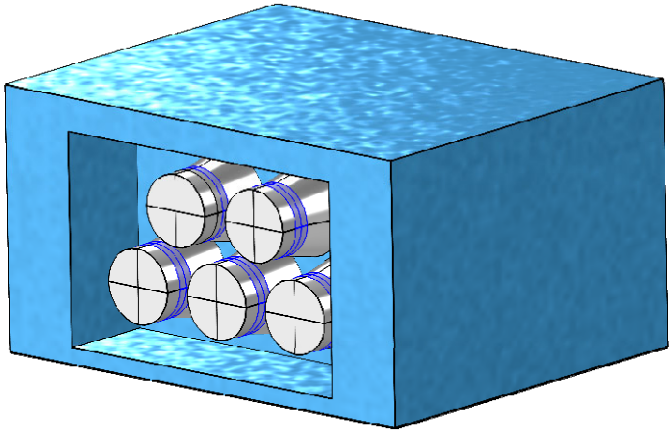

3 Results and discussion

3.1 Modal analysis

It can be seen from Figure 8 of the modal results that the natural frequency of the transducer is about 39.4 kHz. The finding is basically consistent with the theoretically calculated result, which verifies the rationality of the finite element analysis. By analysing the displacement contour of the transducer under resonance, it can be seen that

the amplitude of the front cover of the transducer is about 1.36 mm, the amplitude of the back cover is about 2.46 mm, and the amplitude ratio is 0.55.

From the displacement contour, it can be obtained that in the piezoelectric ceramic area, the displacement is within 0.5 mm, indicating that the deformation of the piezoelectric ceramic is less than 0.5 mm, which meets the design requirements.

Figure 8 The first-order longitudinal vibration of the transducer (see online version for colours)

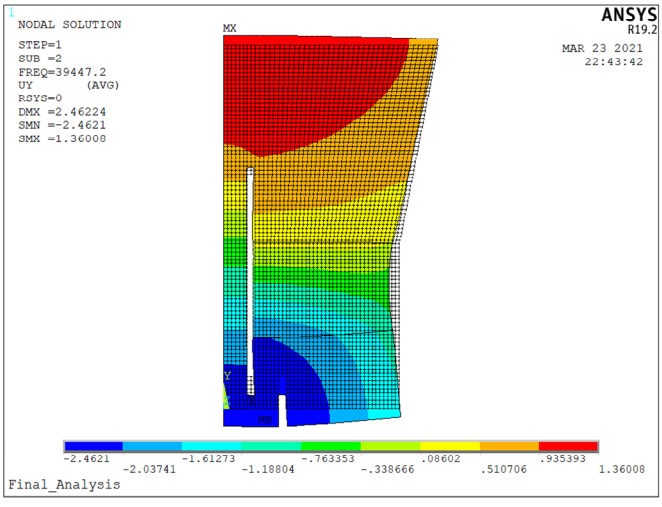

The position of the inner section of the transducer is about y = 21 mm. The interface between the front cover and the piezoelectric ceramic is closer to the front end of the transducer than the theoretical analysis, which is consistent with the inference. The position of the internal joint surface of the pre-stressed bolt is more forward, and the two do not overlap. And the displacement at the nodal plane is not equal to zero but remains a minimal value, indicating that the piezoelectric ceramic also has a certain deformation.

3.2 Harmonic response analysis

Through the analysis of the harmonic response of the transducer, the vibration and electrical performance of the transducer were studied more deeply. Using harmonic response analysis to extract the flowing charge of the piezoelectric ceramic interface during the working process of the transducer, the admittance of the transducer can be calculated (Shang et al., 2016), as shown in Figure 9.

According to Li (2007), the maximum conductance at the fundamental frequency of the transducer can be obtained from the admittance G and B components and the modulus value: G_m =0.13 ms, then the equivalent impedance of the transducer at fundamental frequency resonance is: $R_1 = \dfrac{1}{G_m} = 7.69\ k\Omega$.

In Figure 9(a), the conductance curve has a peak. Obviously, the frequency point corresponding to the peak of the conductance curve is exactly the resonance frequency point of the transducer. From the figure, it can be seen that the frequency corresponding

to this point is 39.41 kHz. There is a peak and a valley in the susceptance curve, which correspond to the first half power point and the second half power point of the resonance point of the transducer (Fan et al., 2021). It can be seen from the susceptance curve that the frequency of the first half power point of the resonance point is f_1 = 39.32 kHz, and the frequency of the second half power point of the resonance point is f_2 = 39.65 kHz. Moreover, the following parameters can be obtained:

- Transducer –3 dB bandwidth: $f_2 - f_1 = 0.33$ kHz, then the mechanical quality factor:
$$Q = \frac{f_r}{f_2 - f_1} = 119.42.$$
- Electromechanical coupling coefficient: $k_{eff}^2 = 1 - \frac{f_r^2}{f_a^2}$, then $k_{eff} = 0.357$.

Generally, the mechanical quality factor of the transducer is between 70–100, and the electromechanical coupling coefficient is about 0.35. It can be seen that the transducer designed and selected in this project meets the requirements of high efficiency.

Figure 9 (a) Conductance and susceptance curve with the frequency (b) Admittance circle diagram (see online version for colours)

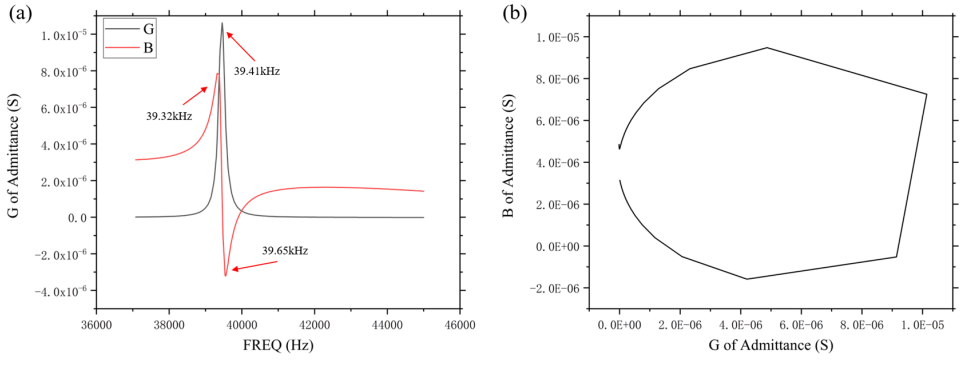

3.3 Sound field analysis

Figure 10 shows the simulated sound pressure distribution in the XY plane. It can be seen that the sound pressure alternates between positive and negative pressures from the centre to the outside. At the same time, because the transducers are arranged in a symmetrical array, the sound pressure also exhibits axisymmetric characteristics.

The simulation is performed by setting the transducer frequency to 28 kHz and 40 kHz, and the extracted sound pressure parameters are shown in Table 4. It can be found that compared to 28 kHz when the transducer frequency is set to 40 kHz, the sound pressure is greatly improved, and the cleaning effect is correspondingly better.

Table 4 The sound pressure parameters

Transducer frequency	P_{max}/Pa	P_{min}/Pa
28 kHz	4.09×10^5	-2.89×10^5
40 kHz	8.38×10^5	-5.57×10^5

Figure 10 (a) Modelling diagram of the water body in the washing machine and the sink (b) Sound pressure distribution diagram (see online version for colours)

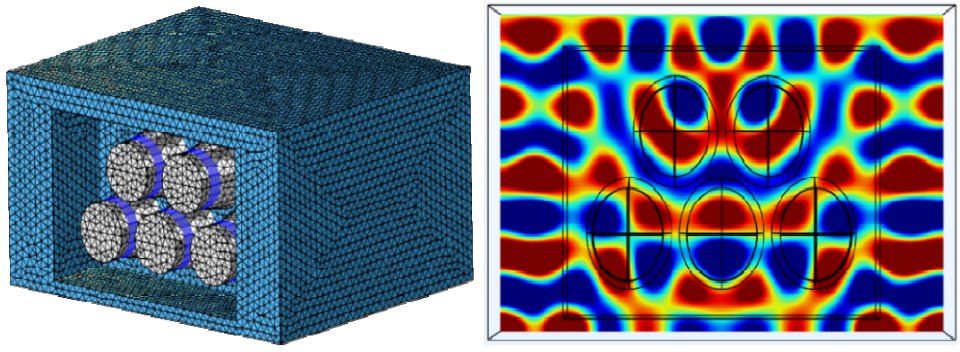

(a) (b)

When the amplitude of the alternating sound pressure is greater than the hydrostatic pressure, negative pressure will be generated. According to Yang et al. (2018), cavitation will only be formed when the negative pressure exceeds the strength of the liquid. The cavitation threshold of water is $P_C = 1.03 \times 10^5$ Pa at 20°C. It can be seen from Figure 11 that when a 40 kHz transducer is used except for individual areas (light yellow, green, and light blue areas), the sound pressure of most areas on the plane (dark red and dark blue areas) is greater than the cavitation threshold ($P_C = 1.03 \times 10^5$ Pa). And when 28k Hz transducer is used, the uniformity of sound pressure distribution and the degree of cavitation are not ideal.

Figure 11 Schematic diagram of the cavitation area at, (a) 28 kHz (b) 40 kHz (see online version for colours)

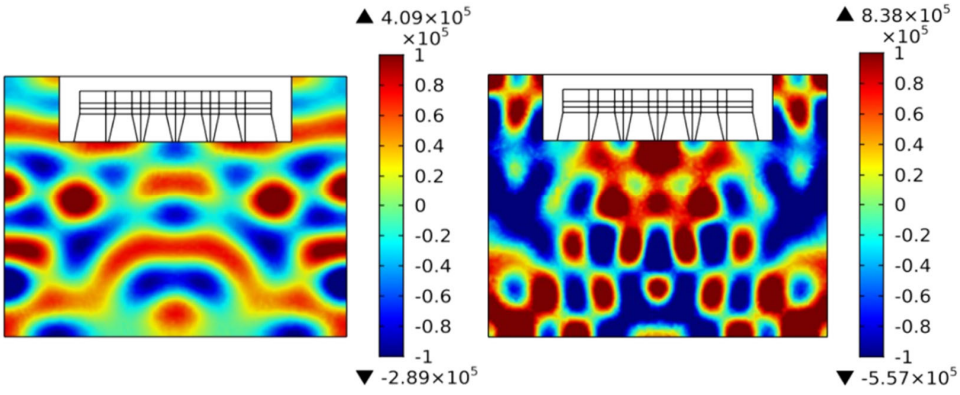

(a) (b)

Meanwhile, it can be found that there are some areas in the transition gap between the two transducers, and the sound pressure value is lower than the cavitation threshold ($P_C = 1.03 \times 10^5$ Pa), which is a blind area for cleaning (Ma and Zhang, 2012). This is caused by standing waves in the sound field, which may affect the consistency of the kitchenware cleaning effect. Methods such as extending the bandwidth of the transducer,

an array of transducers, and changing the posture of the kitchen utensils in the sound field can be used to reduce the influence of standing waves. Through the sound field simulation analysis, it is confirmed that the array pattern of the vibration plate (using five transducers with a frequency of 40 kHz and a power of 300 W) can complete the cleaning work under the static state of the cleaning fluid.

4 Conclusions

Based on the above investigation, the following key conclusions can be obtained.

- Based on the electromechanical equivalent method, the frequency equation of the sandwich piezoelectric transducer was established through the one-dimensional variable cross-section rod vibration equation and combined with the actual engineering requirements of this project. The portable ultrasonic cleaner was designed.
- A two-dimensional axisymmetric finite element model of the transducer was established, and the finite element modal and harmonic response analyses were conducted to obtain critical parameters such as natural frequency, electromechanical coupling coefficient, mechanical quality factor, electrical admittance, etc. The performance of the selected transducer was up to the standard, and the efficiency and accuracy of the finite element simulation method were verified.
- Ultrasonic cleaning has a standing wave effect, which may affect the consistency of the cleaning effect of kitchen utensils. Methods such as extending the bandwidth of the transducer, an array of transducers, and changing the posture of the kitchen utensils in the sound field can be used to reduce the influence of standing waves. Through the sound field simulation analysis, it was confirmed that the array pattern of the vibration plate (using five transducers with a frequency of 40 kHz and a power of 300 W) can complete the cleaning work under the static state of the cleaning fluid.

References

Chang, Z.Y. (2017) *Structural Design and Acoustic Characteristics Analysis of Sandwich Longitudinal Piezoelectric Transducer*, Harbin Institute of Technology.

Duan, Y., Yu, L.Y. and Zou, L. (2018) 'Design of frequency tracking driver of piezoelectric transducer', *Chinese Journal of Sensors and Actuators*, Vol. 31, No. 9, pp.1331–1336.

Fan, Z.L., Zou, D.P., Liu, X., Zhang, C., Yuan, M.D., Zhang, Y.K. and Ye, G.L. (2021) 'Immersion ultrasonic testing for chips substrate materials', *Machine Tool & Hydraulics*, Vol. 49, No. 1, pp.26–30.

Fu, J.P., Shi, P., He, Y.C., Zhang, Y.Z., Liu, Q. and Liang, C.S. (2015) 'Effects of ultrasonic frequency on descaling scope and descaling efficiency', *Chemical Industry and Engineering Progress*, Vol. 34, No. 10, pp.3809–3813.

Fu, M.R., Tang, Y.J. and Chen, M. (2014) 'Equivalent circuit simulation and experimental study on piezoelectric transducer's characteristics near resonance frequency', *Electromachining & Mould*, Vol. 4, No. 1, pp.32–35+40.

Fu, Y., Chen, Y. and Zhang, W.M. (2018) 'Design and optimization of sandwich piezoelectric transducer based on COMSOL multiphysics', *Light Industry Machinery*, Vol. 36, No. 5, pp.1–8+13.

Gonzalez-Avila, S.R., Prabowo, F., Kumar, A. and Ohl, C-D. (2012). 'Improved ultrasonic cleaning of membranes with tandem frequency excitation', *Journal of Membrane Science*, Vols. 415–416, pp.776–783.

Hu, T., Liu, Y. and Fu, B. (2021) 'Design of full wave piezoelectric ultrasonic transducer based on mechanical quality factor', *Technical Acoustics*, Vol. 40, No. 2, pp.286–294.

Kim, T-H. and Kim, H-Y. (2014) 'Disruptive bubble behavior leading to microstructure damage in an ultrasonic field', *Journal of Fluid Mechanics*, Vol. 750, pp.355–371.

Li, J.R. (2007) 'Study on admittance circle diagram of piezoelectric ultrasonic wave transducer', *Instrumentation Technology*, Vol. 4, No. 11, pp.62–64.

Li, X., Song, Y.P., Wang, Z.B., Yang, C.Q., Xue, R., Yu, H. and Wu, C.C. (2016) 'The analysis of a piezoelectric transducer equivalent impedance model and the design of an impedance matching circuit', *Journal of Applied Acoustics*, Vol. 35, No. 1, pp.13–19.

Li, Y.Y. (2019) 'Research and design of dual-frequency ultrasonic cleaning and descaling system', *Cleaning World*, Vol. 35, No. 1, pp.15–19.

Lin, S.Y. (2009) 'Foundations of ultrasonic technology – the theory and design of ultrasonic transducers', *Physics*, Vol. 38, No. 3, pp.141–148.

Ma, K., Zhu, X.J., Hu, Y. and Hou, S.H. (2017) 'Simulation of ultrasonic vibration radiated sound field and analysis of its influence on cavitation structure', *Proceedings of the 17th National Special Processing Conference, Special Processing Branch of Chinese Mechanical Engineering Society, Guangdong University of Technology: Chinese Mechanical Engineering Society*, Vol. 6, pp.519–524.

Ma, S.H. and Zhang, X.J. (2012) 'Working parameters optimization of ultrasonic cleaning machine for jujube', *Transactions of the Chinese Society of Agricultural Engineering*, Vol. 28, No. 15, pp.215–220.

Mason, W.P. (1956) 'Physical acoustics and the properties of solids', *Journal of the Acoustical Society of America*, Vol. 28, No. 6, pp.1197–1206.

Mo, X.P. (2007) 'Simulation and analysis of acoustics transducers using the ANSYS software', *Technical Acoustics*, Vol. 6, pp.1279–1290.

Shang, Y.H., Zhang, Z.Q. and Fang Y.J. (2016) 'Design and development of III type flextensional transducer', *Piezoelectrics & Acoustooptics*, Vol. 38, No. 4, pp.575–578.

Shi, Y. and Yang, Y.J. (2011) 'Design of quarter wavelength sandwich piezoelectric ceramic ultrasonic transducer', *Tool Engineering*, Vol. 45, No. 3, pp.72–74.

Wang, G.S. and Chen, H.J. (2018) 'Research on electromechanical conversion coefficient of the piezoelectric transducer', *Piezoelectrics & Acoustooptics*, Vol. 40, No. 2, pp.247–250.

Wang, W.H. and Du, H.L. (2019) 'Development of automatic ultrasonic industrial cleaning machine', *Machine Tool & Hydraulics*, Vol. 47, No. 2, pp.49–53.

Xu, B., Li, A.J., Li, X.F. and Zhang, J.H. (2018) 'Effects of the shape of sandwich piezoelectric transducer on its vibration performance', *Metrology & Measurement Technique*, Vol. 45, No. 8, pp.45–49.

Xu, L. and Cheng, Y.B. (2020) 'Optimization of the sandwich piezoelectric ultrasonic welding transducer', *Journal of Shaanxi Normal University (Natural Science Edition)*, Vol. 48, No. 3, pp.55–59.

Yang, F., Zhang, M.D., He, Q. and Tan, A.Q. (2018) 'The dynamic mechanism of ultrasonic cavitation field distribution', *Journal of Northwest University (Natural Science Edition)*, Vol. 48, No. 1, pp.37–40.

Zhang, C., Dong, S.M. and Liu, T.M. (2020) 'Simulation of radial vibration characteristics of piezoelectric ceramic composite ultrasonic transducer', *Journal of Vibration and Shock*, Vol. 39, No. 21, pp.217–225+240.

Zhang, G. (2009) 'Multifunctional and portable cleaning hand stick for civil use applied ultrasonic wave', *Natural Science Journal of Harbin Normal University*, Vol. 25, No. 6, pp.75–77.